An Implantable RFID Sensor Tag toward Continuous Glucose Monitoring

Zhibin Xiao, Xi Tan, Xianliang Chen, Sizheng Chen, Zijian Zhang, Hualei Zhang, Junyu Wang, Yue Huang, Peng Zhang, Lirong Zheng, and Hao Min

***Abstract*—This paper presents a wirelessly powered implantable electrochemical sensor tag for continuous blood glucose monitoring. The system is remotely powered by a 13.56-MHz inductive link and utilizes an ISO 15693 radio frequency identification (RFID) standard for communication. This paper provides reliable and accurate measurement for changing glucose level. The sensor tag employs a long-term glucose sensor, a winding ferrite antenna, an RFID front-end, a potentiostat, a 10-bit sigma-delta analog to digital converter, an on-chip temperature sensor, and a digital baseband for protocol processing and control. A high-frequency external reader is used to power, command, and configure the sensor tag. The only off-chip support circuitry required is a tuned antenna and a glucose microsensor. The integrated chip fabricated in SMIC 0.13-μm CMOS process occupies an area of 1.2 mm$\times$2 mm and consumes 50 μW. The power sensitivity of the whole system is -4 dBm. The sensor tag achieves a measured glucose range of 0–30 mM with a sensitivity of 0.75 nA/mM.**

***Index Terms*—13.56 MHz, electrochemical sensor, glucose monitoring, implantable, potentiostat, radio frequency identification (RFID), sensor tag, sigma-delta analog to digital converter (sigma-delta ADC), wireless.**

I. Introduction

THE overall number of diabetic patients is currently about 200 million and it is estimated that this number will reach 330 million by 2025 [1]. A number of complications caused by diabetes will bring serious damages to human beings. Long periods of hyperglycemia or hypoglycemia represent a major issue in diabetes therapy since they can cause sudden coma and brain damage [2]. Such complications can be prevented or retarded by controlling the glucose level. Due to the fact that glucose levels in blood can change rapidly (0.125 mM/min), the enzyme-based finger-picking tests often fail to detect all hypoglycemic and hyperglycemic events. Compared with the conventional point-in-time glucose measurements, automated and continuous glucose monitoring can obtain reliable and detailed information about the changing glucose level of diabetic patients. This way, it can help make the early diagnosis and assist in making the best treatment decisions [3].

The integration of sensors into passive RFID tags has recently caused extensive interest among the RFID community. RFID systems are wireless identification systems containing readers and tags. Different from active tags, passive tags can wirelessly communicate with a reader without a battery. The reader powers the tag by transmitting electromagnetic waves and enables it to send back information stored on the chip. Sensor tags have been used in a wide range of applications, from environmental monitoring to personal biomedical uses, such as temperature detection and health monitoring [4]. Due to the problems associated with a battery in sensor tags [5], passive RFID is used for power and data transmission between an implantable passive sensor tag and an external reader. The combination of integrated circuit chips, telecommunications, and micromachined sensors makes it possible to develop a small-size wireless implantable system.

In wireless power transmission, two coils that are inductively or magnetically coupled are used. One is connected to an external reader and the other is connected to the implantable sensor tag. The near-field coils transmit an radio-frequency (RF) signal to provide the required power for the sensor tag system. The frequency ranges of RFID in international standards are from 135 kHz to 2.45 GHz [6]. On one hand, higher carrier frequency can provide high data transmission rates. However, in an implantable system, the tissue absorption coefficient increases for higher frequencies, causing most of the transmitted power to be absorbed by the tissue. On the other hand, the carrier frequency cannot be too low. Otherwise, the tag coil would have to be quite large and also RF burn in the tissue could be a concern. Therefore, a carrier frequency operating at Industrial Scientific and Medical band of 13.56 MHz is selected.

The research for developing a continuous blood glucose monitoring system was started in the early 1960s [7]. A reliable glucose sensor is a main challenge for glucose detection in the previous implantable systems [8]–[12]. The performance of a glucose sensor includes accuracy, sensitivity, response time, and chemical stability (long-life) *in vivo*. In an implantable passive sensor system, it is also a challenge to perform glucose measurement in relevant *in vivo* conditions for needed periods of time. Various

Manuscript received November 1, 2014; revised February 4, 2015; accepted March 16, 2015. Date of publication March 23, 2015; date of current version May 7, 2015. This work was supported in parts by the National Science & Technology Pillar Program of China (2015BAK36B01), the National Natural Science Funds of China (61076022, 61211140046) and the Shanghai Pujiang Program. (Corresponding author: J. Wang).

Z. Xiao, X. Tan, X. Chen, S. Chen, Z. Zhang, H. Zhang, J. Wang, L. Zheng, and H. Min are with the State Key Laboratory of ASIC & System, Fudan University, 200433 Shanghai, China (e-mail: 13110720059@fudan.edu.cn; tanxi@fudan.edu.cn; 12210720120@fudan.edu.cn; 13210720132@fudan.edu.cn; 12210720166@fudan.edu.cn; 12210720161@fudan.edu.cn; junyuwang@fudan.edu.cn; lrzheng@fudan.edu.cn; hmin@fudan.edu.cn).

Y. Huang is with the Department of Electrical and Computer Engineering, Michigan State University, East Lansing, MI 48824, USA (e-mail: huangyue@msu.edu).

P. Zhang is with the Center for Medical Research and Innovation, Shanghai Pudong Hospital and Fudan University Pudong Medical Center, 201399, Shanghai China (e-mail: zhangpg@yahoo.com).

Color versions of one or more of the figures in this paper are available online at http://ieeexplore.ieee.org.

Digital Object Identifier 10.1109/JBHI.2015.2415836

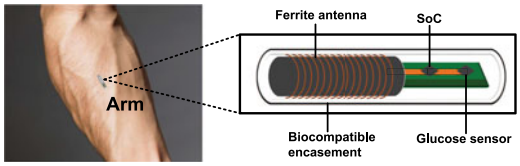

Fig. 1. Wireless powered implantable sensor tag for continuous glucose monitoring. The microsystem includes a ferrite antenna, a system-on-chip (SoC), and an electrochemical glucose sensor.

kinds of glucose sensor systems were successful by using micro/nanotechnologies. On one hand, some of them are based on optical techniques such as near-infrared spectroscopy or light scattering [8], [10]. On the other hand, some methods try to achieve reliable measurements based on electrochemical glucose sensors, which measure the glucose concentration of the interstitial fluid of the skin or other sites. An electrochemical glucose sensor is integrated on chip and the wireless glucose monitoring system consumes about 110 μA [11]. A contact-lens mounted glucose sensor was reported to measure tear glucose. However, time delay and correlation between tear and blood glucose is uncertain [9]. The smallest size microsystem for continuous glucose monitoring is designed and consumes about 6 μW. However, the efficiency of on-chip antenna is much lower and glucose sensors are not sufficiently accurate using a conventional CMOS microfabrication process [12]. Compared with the method that analyzes the various light reflections to measure the glucose level, electrochemical sensors have advantages including avoiding optical interference and can measure electrical signal directly with no large area optical device.

In this paper, we present a wireless powered, long-term implantable sensor microsystem based on RFID for real-time glucose monitoring (see Fig. 1). The microsystem includes an electrochemical glucose sensor, a ferrite antenna, a high-frequency (HF) front end, a digital baseband, and a sensor interface circuit. The sensor tag can detect the glucose level and wirelessly transmit the sensor data to an external reader. This sensor tag system can be seen as a low-cost long-term glucose monitoring device.

In the following sections, the design considerations and the system architecture are described in Section II. Then, the circuit design and implementation are presented in Section III. In Section IV, the experimental results of the sensor tag system are shown, followed by the conclusion in Section V.

II. System Architecture

A. Design Consideration

An implantable glucose sensor tag system including an antenna, a glucose sensor and its interface circuits can be implanted underneath the skin. The implantation site is targeted to be about 3 mm in the subcutaneous tissue where the sensor tag can be in contact with interstitial fluid. The glucose content can have a good correlation with the blood glucose concentration [13]. The communication distance between the sensor tag and a reader is typically 1 cm. The distance is determined by the coupling efficiency of near-field coils, the power conversion efficiency of the HF front end, and the power consumption of the sensor tag system. There are several practical challenges, which should be considered. First, the system uses a 13.56-MHz carrier frequency for RF inductive power. The challenges in an integrated RF energy harvesting system include designing an efficiency rectifier, a low-power regulator, and a large on-chip storage capacitor. Second, normal glucose level in human blood level is 4 mM to 7 mM. In the design, the electrochemical sensor generates current in the order of nA in a reasonable range of 0–30 mM glucose levels for all hypoglycemic and hyperglycemic events. The weak current is easily interfered by different noise sources, such as the supply noise and environment noise. Therefore, accurate detection of a weak current signal requires a stable supply voltage, a reference voltage, and a low noise sensor interface circuit. Third, the size of sensor tag is a key issue in the success of the implantable monitoring system. A small-size system can be packaged and be implanted by invasive surgery. Therefore, for cheaper cost and a longer *in vivo* monitoring lifetime, it becomes more important to reduce off-chip components and minimize the active area of the integrated interface chip. Finally, when a sensor system is to be implanted in body, some other issues should be taken into account, such as biocompatible package material and the effects of the body's immune system and so on. More details about the implantable issues can be found in [11].

B. System Architecture

Fig. 2 shows the overall architecture of wireless powered, long-term implantable sensor microsystem based on RFID technology. The sensor tag integrates an RF front end, a digital baseband, glucose, and temperature sensors readout circuits. In wireless power transmission, two coils that are inductively coupled are used. One is connected to an external reader and the other is connected to the implantable sensor tag.

The front end is mainly responsible for wireless energy harvesting and data transceiver. It receives external RF power through a tuned *LC* matching circuit, followed by a voltage rectifier to generate a dc supply voltage for the whole system.

The sensor readout circuit is designed based on switched-capacitor circuit technology. Through digital switches and selection, the sensor readout circuit can be reconfigured by reader commands to convert different types of signals including glucose sensor and temperature sensor to voltage output. The output voltage is digitalized by 10-bit sigma-delta analog to digital converter (ADC). The signals from two sensors are processed by the same readout circuits to minimize the power and size.

The digital baseband decodes the commands from a reader and manages the operation of the microsystem.

III. Circuit Design and Implementation

A. Near-Field Antenna Design

Implantable applications require small coils for wireless power and data transmission. Since the coil structure affects quality factor (Q), coupling coefficient (K), and inductance, it must be carefully picked to suit the implanted devices. Typical dimension for cylinder coils are $d \times l = 5 \times 0.75$ mm. The

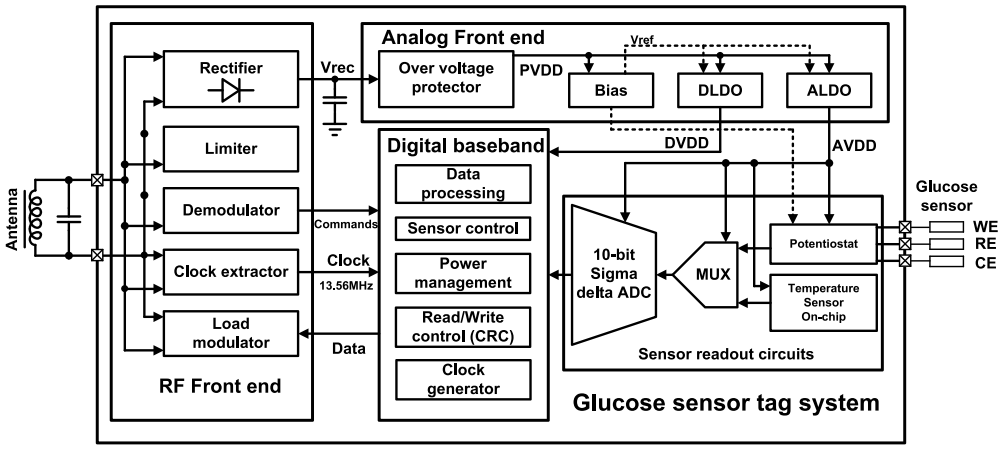

Fig. 2. Block diagram of the wireless sensor tag architecture.

mutual inductance that is decisive for the power supply of the transponder falls sharply due to its proportionality with the cross-sectional area of the coil. For an implantable sensor tag, a ferrite antenna is used for the near-field inductive link. By inserting a ferrite material with a high permeability μ into the coil, the mutual inductance can be significantly increased, thus compensating for the small cross-sectional area of the coil. The quality factor and coupling coefficient of the sensor tag and external reader coils are optimized to achieve the maximum power transfer efficiency so that sufficient energy is powered to the microsystem. The inductance of a ferrite antenna [14] can be calculated according to following equation:

$$L = \frac{\mu_0 \mu_e A \cdot N^2}{l} \tag{1}$$

where μ_0 is the permeability of vacuum, μ_e is relative permeability of ferrite material, N is turns of coil, A is the effective cross-sectional area of ferrite material, l is the effective magnetic path length of ferrite material, and L is the inductance of antenna coil with ferrite material.

B. Energy Harvesting and Load Modulation

In the wireless passive sensor tag, a rectifier is designed to rectify the received RF signal and to charge up a storage capacitor to an unregulated dc supply voltage. A three-stage high-efficiency differential CMOS rectifier with an active threshold voltage (V_{th}) cancellation technique [15] is designed for RF energy harvesting. Power conversion efficiency (PCE) is important for wirelessly powered implantable application, considering the power loss in the human tissue. Experimental tissue attenuation can be obtain from [16]. The attenuation of 13.56-MHz electromagnetic wave in tissue is about 10% when the thickness of tissue is assumed to be 5 mm.

The rectifier can automatically minimize the effective V_{th} of diode-connected MOS transistors in a forward bias condition and increase it in a reverse bias condition by a cross-coupled differential circuit configuration. The differential rectifier reduces both the effective ON-resistance and the reverse-leakage current, and simultaneously, achieves a high PCE, especially under small RF input power. A peak power efficiency of the rectifier is approximately 45% with 30 kΩ load. At the same time, a limiter [17] is employed to clamp the input power and keeps the rectifier output voltage below 1.8 V in case that the tag is exposed to a high strength field.

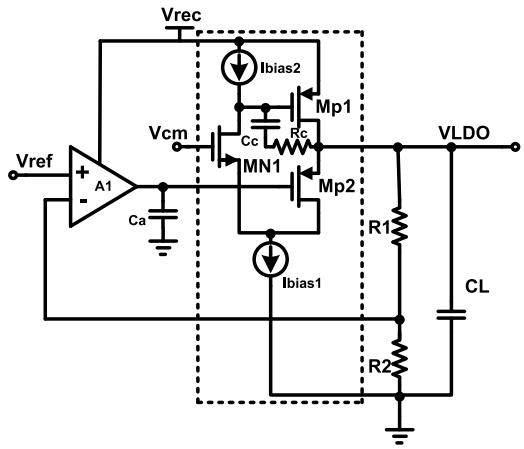

Fig. 3. Schematic diagram of the on-chip regulator.

Load shift key (LSK) is used to transmit the sensor data back to the reader. Modulated reflection is achieved by varying the load impedance of the passive wireless link, which is equivalent to the RF front end input impedance of the sensor tag system. The reader may use the variation of the voltage to decode the backward link signals.

C. Voltage Regulator

The voltage regulator is an important circuit in wireless implantable application. The regulator should produce a clean and stable supply voltage. Since the power received by the sensor tag is limited, a low-power low-dropout regulator (LDO) is required. Fig. 3 shows the schematic of the regulator. Stability enhanced low-dropout regulators are design to adapt varying load current in different work status. To minimize the interference from digital circuits into analog circuits, ALDO and

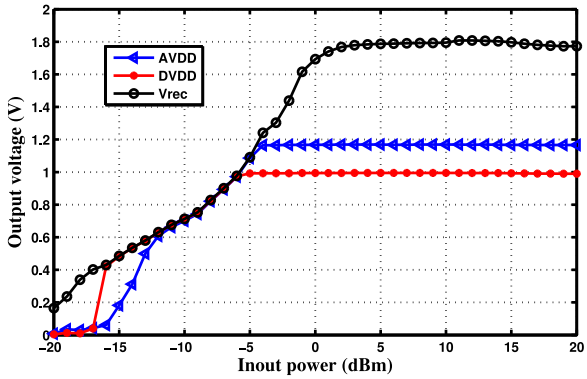

Fig. 4. Measured output voltage of rectifier and regulator versus different input power (a limiter clamps the voltage below 1.8 V).

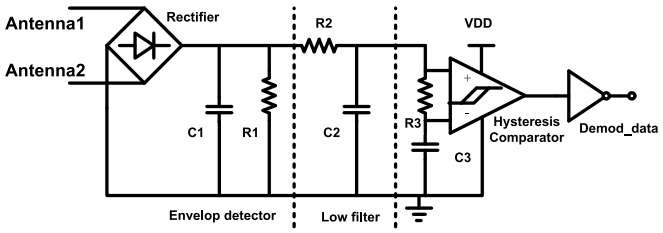

Fig. 5. Block diagram of the demodulation circuit.

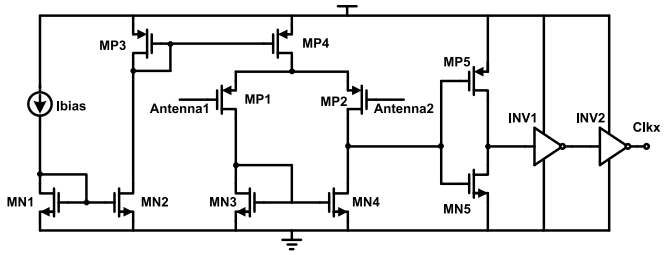

Fig. 6. Schematic diagram of the clock extractor.

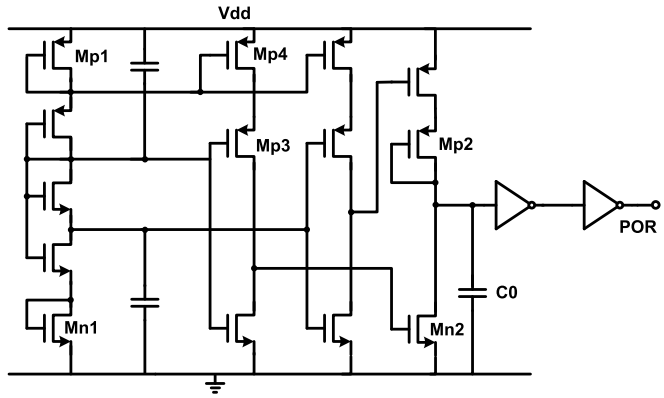

Fig. 7. Schematic diagram of the POR.

DLDO are designed for analog and digital circuits, respectively. Separated regulators provides 40-dB isolation between analog and digital circuits. The supply voltage for digital circuits is set to 1 V, which reduces dynamic power by 30% compared with 1.2 V. The LDOs use a flipped voltage follower [18] as an output stage to improve load regulation and avoid requiring a large decoupling capacitor. Fig. 4 shows the measured output voltage of rectifier and regulator versus different input RF power.

D. Demodulation

An ASK demodulator [19] is commonly used to demodulate the commands data from an external reader at low data rate. As shown in Fig. 5, it is composed of a voltage rectifier, a diode envelope detector, a low-pass filter, an average detector, and a comparator. As the received signal strength may vary when the distance between the reader and the sensor tag, a dynamic reference threshold for comparison is required. The dynamic threshold is given by the average value of the envelope. Average generation is obtained with an integrated *RC* filter. The demodulator can demodulate a minimum input signal level of 100 mV at a data rate of 26.5 kbps and a modulation depth from 10% to 100%.

E. Clock Extraction and POR Generation

For an HF tag system, it is easy to extract the clock from the carrier wave. The reason is that the data rate compared to the carrier frequency is not small in the HF system. When the circuit is implemented, two problems must be considered. First, since the input of the clock extraction is an antenna, the ASK modulation will cause the amplitude to drop very low. Second, during the load backward modulation, the antenna amplitude will also be dragged to low, so it is important to maintain the clock extraction output for small RF signal level. Fig. 6 shows the clock extraction circuit, which consists of a high bandwidth differential comparator and following inverters. The 13.56-MHz clock is extracted from the carrier and directly fed into the digital baseband. The circuit can extract the clock from a minimum of 50-mV amplitude signal from the antenna.

Power on reset (POR) has two major functions. One is to generate the whole chip reset signal when the sensor tag is powered up by HF electronic magnetic field. The other is to protect the chip circuit from malfunction when the supply voltage drops under a certain level. The critical problem is the power consumption of the POR circuit itself. Fig. 7 shows a low power POR circuit. The quiescent current is less than 100 nA. MP2 and C0 form the delay circuit to generate the delay time needed to ensure a reliable stable supply.

F. Potentiostat

Amperometric electrochemical sensors are able to generate a current linearly proportional to glucose concentration and typically consist of three electrodes namely the working, reference, and counter electrodes (WE, RE, and CE, accordingly). The active area of glucose sensor in this system is 0.15 mm^2 and the sensor sensitivity is 0.01 $\mu A \cdot mm^{-2} \cdot mM^{-1}$ when the glucose concentration is in the range of $0 \sim 30$ mM. The needed sensitivity for practical *in vivo* applications depends on application requirements and the features of sensor systems. Glucose oxidase (GOD) enzyme and glucose permeable membrane are

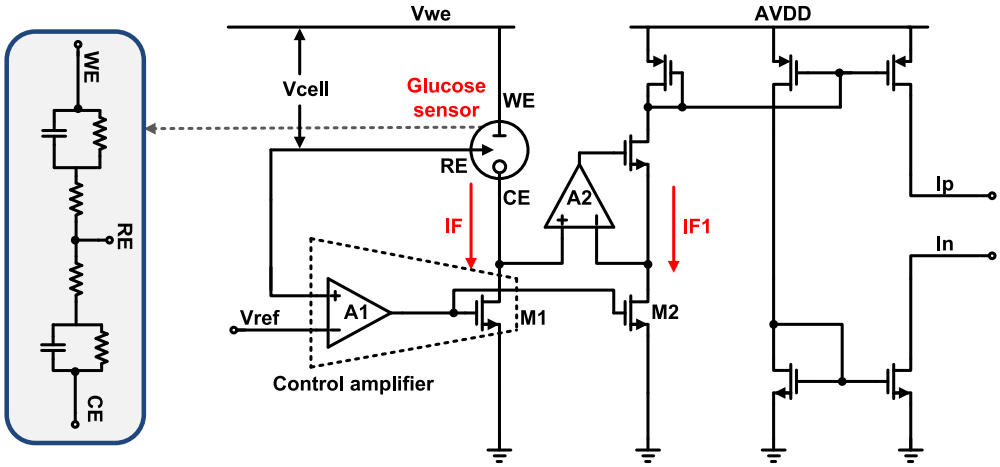

Fig. 8. Schematic diagram of the current mirror-based potentiostat.

used to create a glucose sensitive layer on the WE area. This glucose sensitive layer rejects water molecules through a semipermeable membrane and allows glucose molecules through it. The ratio of glucose molecules versus water molecules is about 50:1. The number of sensing electrons is effectively reduced in the entire redox process, greatly reducing the required potentiostat operating voltage. More importantly, it improves the lifetime of the electrochemical sensor. In this design, the sensing current accuracy is 0.1 nA. The 0.01 $\mu\text{A} \cdot \text{mm}^{-2} \cdot \text{mM}^{-1}$ sensitivity glucose sensor generates current around 0–20 nA in a reasonable range of 0–30 mM glucose levels. The narrow dynamic current range reduces complexity of the sensor interface circuits including the potentiostat and the ADC to minimize the power and size. From an electronic standpoint, an electrochemical sensor can be regarded as a network of impedances and active elements. Fig. 8 shows the small signal equivalent circuit of an electrochemical sensor [20].

A current mirror-based potentiostat is designed (see Fig. 8). It is composed of two main subcircuit. The conventional potential control loop guarantees a fixed potential between the WE and RE (*V*cell, 200 mV in this design). In order to maximize the stability of the potential-control loop, A1 should be a single-stage amplifier that introduces only one low-frequency pole into the loop. The double-layer capacitance of the electrode interface is very large, which is the dominant pole of this loop [21]. To achieve good loop stability, the first nondominant pole is pushed to high frequencies (the pole of A1, in this design). A current mirror with a high gain error cancellation is designed, by adding the operation amplifier A2 to mirror the sensor output current IF to IF1 accurately. The current mirror isolates the potentiostat and the measurement circuits that release design constrains for both sides. The copied current IF1 is translated into differential current I_p and I_n to resist the common mode interference.

To measure the accuracy of the on-chip potentiostat, a commercial potentiostat is used to measure and calibrate the output current of the glucose sensor at the same time. Fig. 9 shows the measured differential output current of the current mirror versus the calibrated sensor output. The liner correlation coefficient is 0.999936.

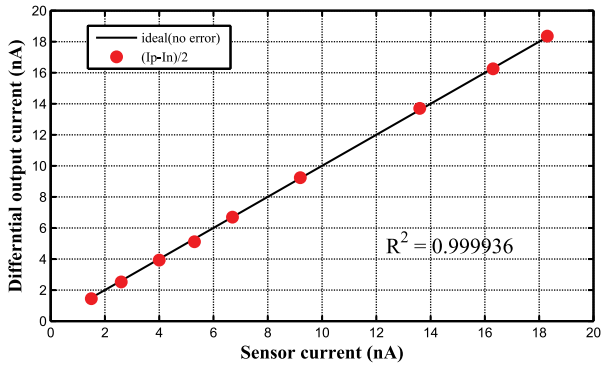

Fig. 9. Measured potentiostat differential output current versus sensor current.

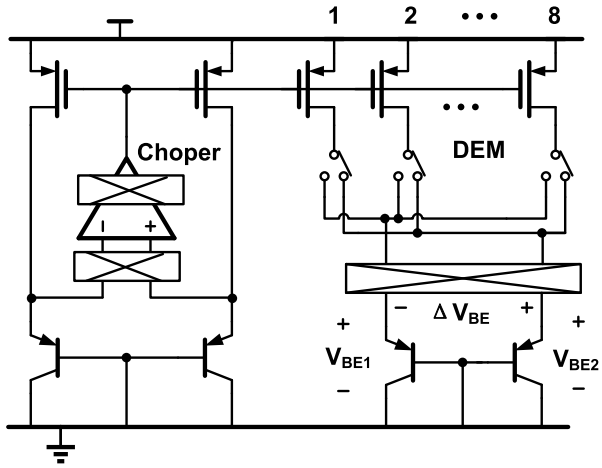

Fig. 10. Schematic diagram of the on-chip temperature sensor.

G. Temperature Sensor

The glucose sensor in this study has a temperature coefficient around 1 nA/°C, so a bipolar junction transistor (BJT)-based temperature sensor is integrated to provide real-time temperature data for reference, as shown in Fig. 10. For body temperature sensing from 32 °C to 42 °C, necessary dynamic

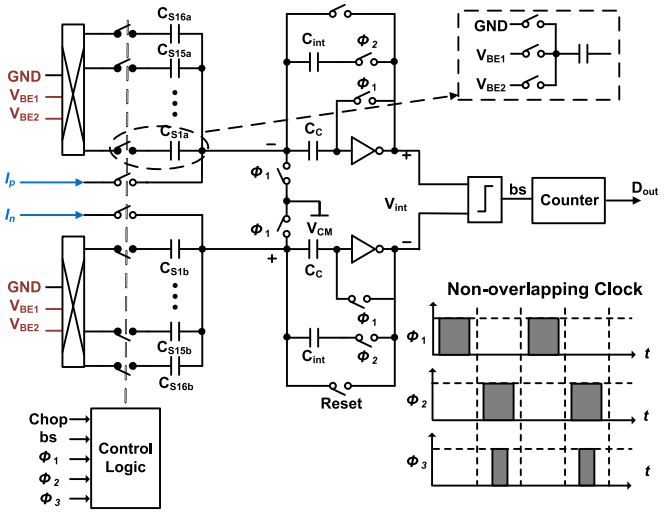

Fig. 11. Schematic diagram of the sigma delta ADC.

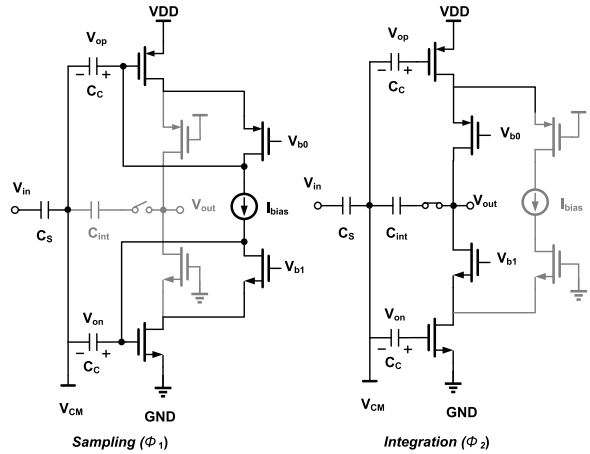

Fig. 12. Schematic diagram of the inverter-based OTA.

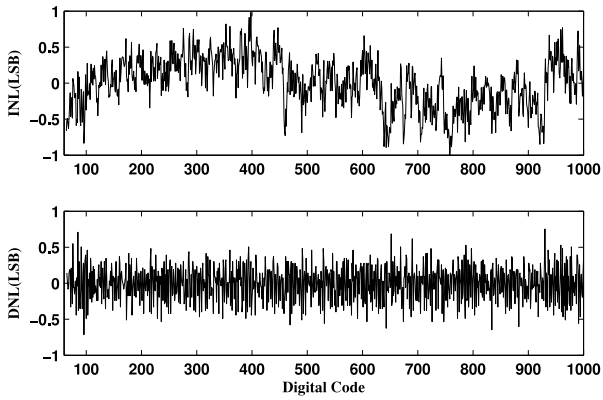

Fig. 13. Measured the 10-bit sigma-delta ADC static characteristic.

range of the ADC is about 7-bit to reach 0.1 °C resolution. The temperature sensor can also be used outside the body. Therefore, for a reasonable temperature range from 20 °C to 50 °C, the ADC should have at least a 9-bit dynamic range to achieve 0.1 °C resolution. From the temperature-dependent ratio of bipolar transistors: where $V_{\rm BE}$ is the base-emitter voltage and $\Delta V_{\rm BE}$ is the $V_{\rm BE}$ difference between two transistors (in this design, k varies from 11 to 13 over temperature range from 20 °C to 50 °C), a linear temperature coefficient can be used to indicate the temperature

$$\mu = \frac{\alpha \cdot \Delta V_{\rm BE}}{V_{\rm BE} + \alpha \Delta V_{\rm BE}} = \frac{\alpha}{V_{\rm BE}/\Delta V_{\rm BE} + \alpha} = \frac{\alpha}{K + \alpha} \qquad (2)$$

where α is a gain factor, which can be trimmed to compensate for $\Delta V_{\rm BE}$ spread [22]. Chopping and dynamic element matching technology [23] is used to suppress mismatch and process variations.

H. Sigma-Delta ADC

A 10-bit differential low-voltage low-power incremental sigma-delta ADC (see Fig. 11) is designed to digitize the output of both the glucose sensor and the temperature sensor (in time division, configured by reader commands). The differential structure provides both rejection to common mode interference, suppression to clock feed, and charge injection. Pseudodifferential inverter-based integrators [24] are used in the ADC, achieving a minimum operation supply voltage of 0.85 V and 3 μW-power consumption at 214-kHz switching frequency. Unfortunately this integrator is of the sensitive PVT variation and suffers from bad 1/f noise and offset performance. Dynamic current biasing and autozeroing techniques are introduced to overcome these drawbacks.

Fig. 12 shows the inverter-based amplifier, which draws 400 nA and has a dc gain of 80 dB. Fig. 13 shows the 10-bit ADC static characteristic, achieved with 0.6-LSB INL and 0.8-LSB DNL at 214-kHz switching frequency.

I. Digital Baseband

The digital baseband (see Fig. 14) realizes signal processing, as well as generating the clocks and control signals for the sensor interface circuit and sigma-delta ADC. The digital baseband is mainly divided into eight modules: 1) the clock generator module (CGM) is to divide clocks from 13.56 MHz; 2) the demodulator module is to demodulate commands; 3) the control unit (CU) is to decode commands from the reader; 4) the fist input fist output (FIFO) is to store data from the sigma-delta ADC for sending out when data ready register is set; 5) the sensor control (SC) is to generate control signals for the system; 6) the cyclic redundancy check (CRC) is to detect error and guarantee the data integrity; 7) the modulation module (MOD) is to send sensor data to a reader by load modulation; and 8) the power management module (PMW) is to manage the power and distribute the clocks of the system.

The operation of the sensor tag is able to be controlled between different states by user commands. The air interface is complied with the ISO 15693 standard. The tag supports inventory, and write and read commands. The sensor tags are uniquely identified by a 64-bit Unique Identifier (UID). The UID is used to address each sensor tag uniquely and individually, during the anticollision loop and for one-to-one exchange between a sensor tag and the reader. The external reader can write configuration

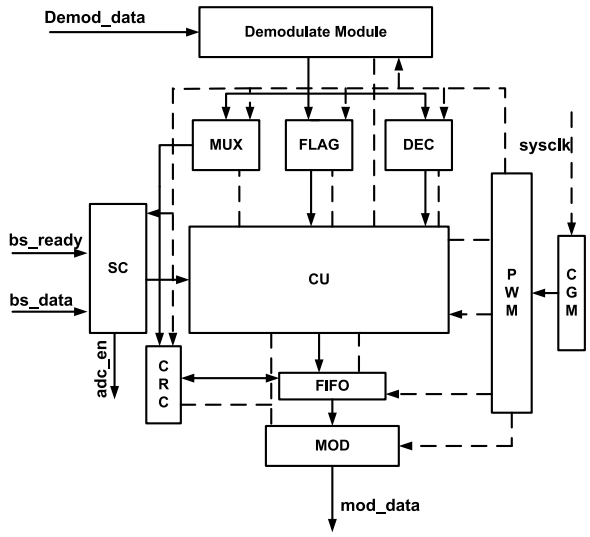

Fig. 14. Block diagram of the digital baseband.

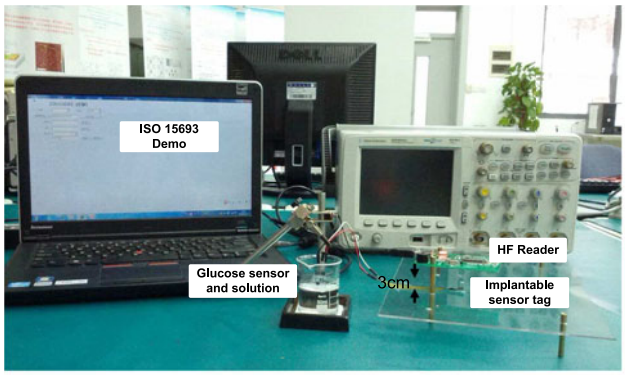

(a)

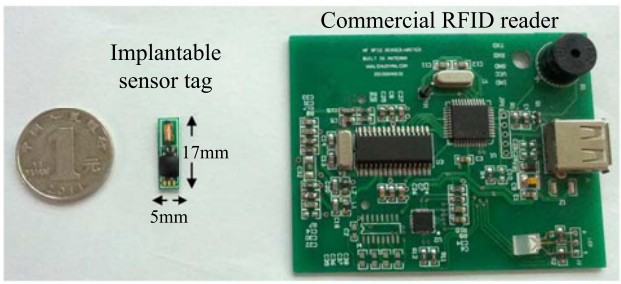

(b)

Fig. 15. (a) Measurement setup of the sensor tag and wirelessly measured glucose readout data in-vitro experiment. (b) Photograph of the packaged device for long-term implantable glucose monitoring and external HF reader.

information to the sensor tags. Such information can provide maximum flexibility for the sensor to work and for the reader to obtain data from the sensor tag.

The operation states of the sensor tag system mainly include receiving, processing, and transmitting. The state machine controls the operations of the sensor tag system. When it receives the carrier signal, the sensor tag goes to the receive state after the baseband is reset by a POR signal and the clock is generated. After the inventory request command, an UID is transmitted

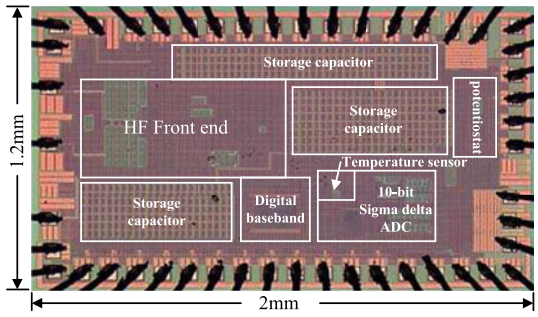

Fig. 16. Chip microphotograph of the proposed circuits.

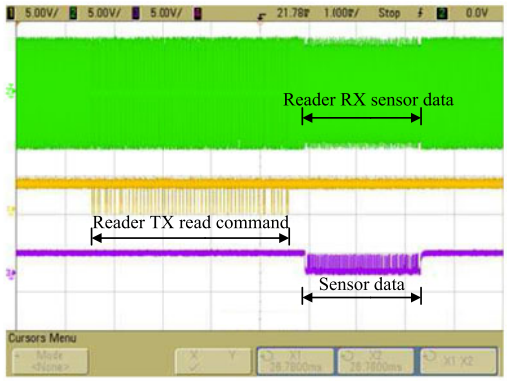

Fig. 17. Measured waveforms of the demodulated command, backscattered sensor data by load modulation, and voltage of reader antenna.

back to reader. After the sensor tag is uniquely identified by the UID, the reader can send operation instructions and configuration information by a write command. Various clocks and control signals are generated to control the sensor interface and the sigma-delta ADC. The sensor tag then goes to the processing state. After the ADC completes data conversion, the sampled sensor data are written to 32-bit registers and the sensor tag goes to the transmission state. Finally, the reader gets the sensor data by sending a read request command. Data transmission is encoded through a CRC to guarantee the data integrity.

IV. Experimental Results

The proposed circuits for 13.56-MHz sensor tag has been fabricated in the SMIC 0.13-μm 1P8M CMOS technology. Fig. 16 shows the chip microphotograph of the proposed circuits. The chip area including on-chip storage capacitor is only 1.2 mm $\times$ 2 mm and has a power consumption of 50 μW.

In the system testing, a PCB-based tag prototype consisting of an antenna and the fully integrated sensor tag chip, as shown in Fig. 15(b), is connected to the three electrodes of the glucose sensor. The air interface is complied with the ISO15693 standard. In Fig. 15(b), an HF RFID reader is used to communicate with the sensor tag. The potentiostat and the ADC can be separately controlled by writing respective control word to the tag. The energy coupled to the ferrite antenna is converted to dc to supply power to the microsystem. The commands from the reader are demodulated for the system configuration. The

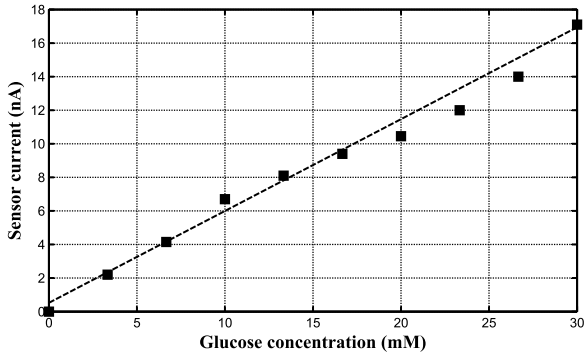

Fig. 18. Measured sensor current versus glucose concentration.

TABLE I
MEASUREMENT PERFORMANCE

Parameter		Performance
Technology		SMIC 1P8M 0.13-μm CMOS
Supply	analog	1.2 V
	digital	1.0 V
Carrier frequency		13.56 MHz
Protocol		ISO 15693 RFID standard
Demodulation scheme		ASK(modulation depth is 10% or 100%)
Modulation scheme		LSK
Active area		1.2 mm $\times$ 2 mm
Power	Total	50 μW
	HF Frontend	28 μW
	ADC	3 μW
	Potentiostat	4 μW
	Digital baseband	15 μW
Efficiency	rectifier	45%(max)
	regulator	90%
Glucose sensor	Area	0.15 mm^2
	Sensitivity	0.01 μA $\cdot$ mm^2 $\cdot$ mM^{-1}
	Glucose level	0–30 mM
	Current range	20 nA
10-bit $\Sigma\Delta$ ADC	Current range	0–40 nA
	ENOB	9.3 bit
	INL/DNL	$\pm$0.6 LSB/$\pm$0.8 LSB
Potentiostat	Linearity (R^2)	0.999936
Temperature Sensor	Type	BJT
	Range	20 °C $-$ 50 °C
	Accuracy	0.5 °C
Implant coil	Ferrite material	NiZn
	Diameter	1.2 mm

clock is extracted from the carrier wave to provide clock to the baseband and divided into a particular clock for the sigma-delta ADC. The demodulator supports a modulation depth of 10% to 100%. The digitized sensor data are sent back by load modulation. The glucose sensor tag can be powered over 3 cm from the external HF reader with an effective isotropically radiated power of 20 dBm at 13.56 MHz in free space. Theoretically, the sensor tag can receive power larger than -4 dBm to power the sensor tag in a distance of about 2.5 cm *in vivo*.

The efficiencies of the rectifier and LDO regulator are measured as 45% and 90%, respectively. The pseudodifferential inverter-based ADC achieves a minimum operation supply voltage of 0.85 V and 3-μW power consumption with less than 0.6-LSB INL and 0.8-LSB DNL at 214-kHz switching frequency.

TABLE II
COMPARISON WITH PRIOR ARTS

	This Study	[10]	[9]	[12]
Carrier Frequency	13.56 MHz	13.56 MHz	2.4 GHz	900 MHz
Protocol	ISO 15693	ISO 15693	N/A	N/A
Modulation scheme	LSK	LSK	LSK	LSK
Noise Cancellation	Auto-zero and chopper	N/A	N/A	N/A
Glucose level	0–30 mM(blood)	0–40 mM(blood)	0–2 mM(tear)	0–20 mM(tissue fluid)
Sensing area (mm^2)	0.15	1.488	0.22	0.24
Glucose sensitivity (μA $\cdot$ mm^{-2} $\cdot$ mM^{-1})	0.01	N/A	1.65	N/A
Measure current range	40 nA	1.16 μA	750 nA	45 nA
Temperature Sensor	Yes	Yes	No	No
Energy sensitivity	-4 dBm	N/A	0 dBm	N/A
Power (μW)	50	250	3	6
Chip size (mm^2)	2.4	9.98	0.5	1.96
Storage capacitor on-chip	Yes	No	Yes	Yes

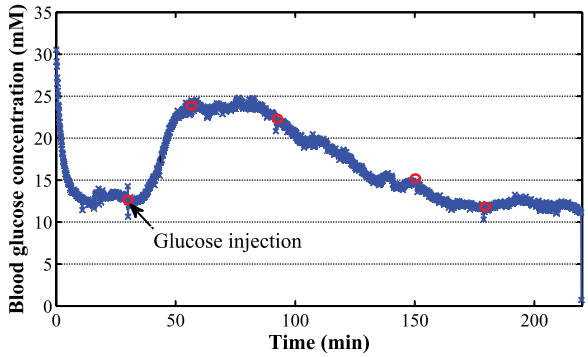

Fig. 19. IPGTT in rats.

In order to test the performance of the proposed sensor tag monitoring system in measuring glucose concentration, a Sigma P-3813 phosphate buffered solution (pH 7.4) with 330-mM NaCl was used. In the human body, normal glucose level is 4–7 mM. This range for diabetic patient, such as hypoglycemic (0–2 mM) and hyperglycemic (10–30 mM), is narrow. Therefore, in our experiment, we increased the glucose concentration of the solution from 0 to 30 mM, by gradually adding glucose to the solution. After settling the sensor current to its final value (in approximately 2 min), the glucose sensor data were measured using the wireless sensor monitoring system.

The measured waveforms of the demodulated command, backscattered sensor data by load modulation, and voltage of the reader antenna are shown in Fig. 17. Fig. 18 shows measured sensor current versus glucose concentration using the wireless sensor tag monitoring system.

Table I summarizes the measured performance of the sensor tag and Table II compares this study with the state-of-art device for continuous glucose monitoring.

A continuous *in vivo* measurement in an animal has already been completed. Three-month old male Wistar rats are employed in this test. An intra-peritoneal glucose tolerance test (IPGTT)

[25] was carried out after a 12-h fasting period. Then, the sensor tag is used for continuous glucose monitoring which lasted for about 4 h. The measured result is shown in Fig. 19. After the intraperitoneal injection of 50% glucose (1 g/kg body weight) at the point of 30 min, the value of blood glucose in rats rises up to 25 mM rapidly. Then, it drops gradually. For the purpose of verification, the blood glucose level is also simultaneously tested by a commercial glucometer at the points of 0.5, 1, 1.5, 2.5, and 3 h. Both glucose excursion match well.

V. Conclusion

Automated and continuous glucose monitoring technical is required both by clinical and patient care. This paper presents an electrochemical-sensor-based, wireless powered implantable microsystem for real-time glucose monitoring. The sensor tag employs an electrochemical sensor, a winding ferrite core antenna, a 13.56-MHz RFID front end, a potentiostat, a 10-bit sigma-delta ADC, an on-chip temperature sensor, and a digital baseband for protocol processing and control. The air interface is complied with the ISO15693 standard. The integrated chip fabricated in SMIC 0.13-μm CMOS process occupies a die area of 1.2 mm $\times$ 2 mm and consumes 50 μW. The highly integrated, low power, simple sensor tag is a low-cost solution for implantable glucose monitoring applications, which are real-time, direct, and accurate. Note that the glucose sensor tag works well in both phosphate buffered solution with added glucose and the animal body. Our future work includes improvement of the system-on-chip performance and clinical tests.

References

[1] International diabetic federation. (2006, Dec.). [Online]. Available: http://www.idf.org/

[2] S. Zimmermann, D. Fienbork, B. Stoeber, A. W. Flounders, and D. Liepmann, "A microneedle-based glucose monitor: fabricated on a wafer-level using in-device enzyme immobilization," in *Proc. 12th Int. Conf. TRANSDUCERS, Solid-State Sens., Actuators Microsyst.*, 2003, vol. 1, pp. 99–102.

[3] F. Ricci, D. Moscone, and G. Palleschi, "Ex vivo continuous glucose monitoring with microdialysis technique: The example of glucoday," *IEEE Sens. J.*, vol. 8, no. 1, pp. 63–70, Jan. 2008.

[4] A. Vaz, A. Ubarretxena, I. Zalbide, D. Pardo, H. Solar, A. Garcia-Alonso, and R. Berenguer, "Full passive UHF tag with a temperature sensor suitable for human body temperature monitoring," *IEEE Trans. Circuits Syst. II, Exp. Briefs*, vol. 57, no. 2, pp. 95–99, Feb. 2010.

[5] T. Akin, K. Najafi, and R. M. Bradley, "A wireless implantable multichannel digital neural recording system for a micromachined sieve electrode," *IEEE J. Solid-State Circuits*, vol. 33, no. 1, pp. 109–118, Jan. 1998.

[6] *IEEE/ISO/IEC Draft Standard for Information Technology—Smart Transducer Interface for Sensors and Actuators—Transducers to Radio Frequency Identification (RFID) Systems Communication Protocols and Transducer Electronic Data Sheet Formats*, P21451-7, pp. 1–91, 2011.

[7] A. Heller, "Implanted electrochemical glucose sensors for the management of diabetes," *Annu. Rev. Biomed. Eng.*, vol. 1, no. 1, pp. 153–175, 1999.

[8] S. Kiseok, H. Unsoo, P. Seongwook, and Y. Hoi-Jun, "An impedance and multi-wavelength near-infrared spectroscopy ic for non-invasive blood glucose estimation," in *Proc. Symp. VLSI Circuits Digest Tech. Papers*, 2014, pp. 1–2.

[9] L. Yu-Te, Y. Huanfen, B. Parviz, and B. Otis, "A 3 uw wirelessly powered CMOS glucose sensor for an active contact lens," in *Proc. IEEE Int. Solid-State Circuits Conf. Digest Tech. Papers*, 2011, pp. 38–40.

[10] A. D. Dehennis, M. Mailand, D. Grice, S. Getzlaff, and A. E. Colvin, "A near-field-communication (NFC) enabled wireless fluorimeter for fully implantable biosensing applications," in *Proc. IEEE Int. Solid-State Circuits Conf. Digest Tech. Papers*, 2013, pp. 298–299.

[11] M. M. Ahmadi and G. A. Jullien, "A wireless-implantable microsystem for continuous blood glucose monitoring," *IEEE Trans. Biomed. Circuits Syst.*, vol. 3, no. 3, pp. 169–180, Jun. 2009.

[12] M. H. Nazari, M. Mujeeb-U-Rahman, and A. Scherer, "An implantable continuous glucose monitoring microsystem in 0.18um CMOS," in *Proc. Symp. VLSI Circuits Digest Tech. Papers*, 2014, pp. 1–2.

[13] E. Kulcu, J. A. Tamada, G. Reach, R. O. Potts, and M. J. Lesho, "Physiological differences between interstitial glucose and blood glucose measured in human subjects," *Diabetes Care*, vol. 26, no. 8, pp. 2405–2409, 2003.

[14] F. Klaus, 'RFID handbook: Fundamentals and applications in contactless smart cards, radio frequency identification and near-field communication," 2010.

[15] K. Kotani, A. Sasaki, and T. Ito, "High-efficiency differential-drive CMOS rectifier for UHF RFIDs," *IEEE J. Solid-State Circuits*, vol. 44, no. 11, pp. 3011–3018, Nov. 2009.

[16] H. Yu, "A wireless microsystem for multichannel neural recording microprobes," Ph.D. dissertation, University of Michigan, Ann Arbor, MI, USA, 2004.

[17] G. K. Balachandran and R. E. Barnett, "A 110 nA voltage regulator system with dynamic bandwidth boosting for RFID systems," *IEEE J. Solid-State Circuits*, vol. 41, no. 9, pp. 2019–2028, Sep. 2006.

[18] P. Hazucha, T. Karnik, B. A. Bloechel, C. Parsons, D. Finan, and S. Borkar, "Area-efficient linear regulator with ultra-fast load regulation," *IEEE J. Solid-State Circuits*, vol. 40, no. 4, pp. 933–940, Apr. 2005.

[19] N. Gay and W. Fischer, "A compact rf / analog front-end for microwave RFID transponders," in *Proc. Semicond. Conf. Dresden*, 2011, pp. 1–4.

[20] M. M. Ahmadi and G. A. Jullien, "A very low power CMOS potentiostat for bioimplantable applications," in *Proc. 5th Int. Workshop System-on-Chip Real-Time Appl.*, 2005, pp. 184–189.

[21] M. M. Ahmadi and G. A. Jullien, "Current-mirror-based potentiostats for three-electrode amperometric electrochemical sensors," *IEEE Trans. Circuits Syst. I, Reg. Papers*, vol. 56, no. 7, pp. 1339–1348, Jul. 2009.

[22] K. Souri, C. Youngcheol, and K. A. A. Makinwa, "A CMOS temperature sensor with a voltage calibrated inaccuracy of 0.15 ºC (3) from -55 ºC to 125 ºC ," *IEEE J. Solid-State Circuits*, vol. 48, no. 1, pp. 292–301, Jan 2013.

[23] G. C. M. Meijer, W. Guijie, and F. Fruett, "Temperature sensors and voltage references implemented in CMOS technology," *IEEE Sens. J.*, vol. 1, no. 3, pp. 225–234, Oct. 2001.

[24] C. Youngcheol, K. Souri, and K. A. A. Makinwa, "A 6.3 uw 20-bit incremental zoom-ADC with 6 ppm INL and 1 uv offset," *IEEE J. Solid-State Circuits*, vol. 48, no. 12, pp. 3019–3027, Dec. 2013.

[25] L. C. Solberg, W. Valdar, D. Gauguier, G. Nunez, A. Taylor, S. Burnett, C. Arboledas-Hita, P. Hernandez-Pliego, S. Davidson, and P. Burns, "A protocol for high-throughput phenotyping, suitable for quantitative trait analysis in mice," *Mammalian Genome*, vol. 17, no. 2, pp. 129–146, 2006.

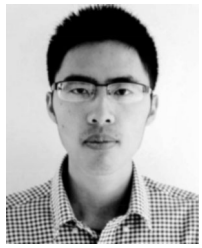

Zhibin Xiao (S'15) was born in Fujian, China, in 1987. He received the B.S. degree in electronic science and technology from National Huaqiao University, Xiamen, China, in 2011, and the M.S. degree in integrated circuit engineering from Fudan University, Shanghai, China, in 2013, where he is currently working toward the Ph.D. degree in microelectronics.

His research interests include low power analog and mixed signal integrated circuit design for wireless implantable sensing applications.

Xi Tan was born Changzhou, China, in 1978. He received the B.S. degree in physics from Nanjing University, Nanjing, China, in 2000, the M.S. degree in microelectronics from the Delft University of Technology, Delft, Netherlands, in 2005, and the Ph.D degree in microelectronics from Fudan University, Shanghai, China, in 2008.

From 2008, he served as an Assistant Researcher of ASIC & Systems State Key Laboratory, and an Associate Director of Auto-ID Lab, Fudan University. He is currently working on the CMOS RF transceiver and system-on-chip for personal communication and UHF band RFID. His research interests include CMOS RF and mixed signal integrated circuit design and wireless communications.

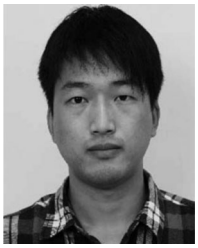

Xianliang Chen received the M.S. degree from the Department of Microeconomics, Xidian University, Xi'an, China, in 2012. He is currently working toward the M.S. degree in the Microelectronics Department, School of Information Science and Engineering, Fudan University, Shanghai, China.

His research interests include sensors interface circuits, precision analog and sigma delta ADC.

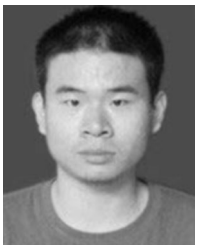

Sizheng Chen was born in Jiangxi, China, in 1991. He received the B.S. degree in electrical science and technology from National Henu University, Henan, China, in 2013. He is currently working toward the M.S. degree in integrated circuit engineering at Fudan University, Shanghai, China.

His research interests include low power analog and potentiostat design for wireless implantable sensing applications.

Zijian Zhang was born in Zibo, China. in 1990. He received the B.S. degree from Shangdong University in 2012. He is currently working toward the M.S. degree in the School of Microelectronics, Fudan University, Shanghai, China.

His research interests include on digital basband design for HF reader and tag.

Hualei Zhang was born in Shanxi, China, in 1989. He received the B.S. degree in integrated circuit design and integrated system from the Xi'an University of Post and Telecommunications, Xi'an, China, in 2012, and the M.S. degree in integrated circuit engineering from Fudan University, Shanghai, China, in 2014, where he is currently working toward the Ph.D. degree in microelectronics.

His research interests include low power analog and RF circuit design for RFID tags application.

Junyu Wang (M'09) was born in Xiangtan, China, on August 14, 1973. He received the Ph.D. degree from the University of Science and Technology, Beijing, China, in 2002.

During 2003–2005, he was a Postdoctoral in Fudan University, Shanghai, China, doing research on anti-counterfeit solutions based on RFID technology. During 2008–2009, he was a Visiting Associate Professor of Massachusetts Institute of Technology, Cambridge, MA, USA, doing research on the security issues and solutions of Internet of Things. He is currently the Associate Director of Auto-ID Lab and an Associate Professor in Fudan University. His research interests include RFID reader and tag design, RFID anticollision algorithm, RFID security, RFID sensor tag, and Internet of Things for food/drug safety.

Yue Huang (S'07) received the B.S. degree in transportation engineering from Southwest Jiaotong University, Chengdu, China, in 1996, and the M.S. degree in electrical engineering in 2007 and Ph.D. degree in electrical engineering in 2011, both from Michigan State University, East Lansing, MI, USA.

His research interests include several aspects of enzyme-based integrated biosensors, including digital/analog integrated circuits, biochemistry, electrochemistry, microfabrication, microfluidics, and microelectromechanical systems.

Dr. Huang is currently a Senior Research Associate, Michigan State University, East Lansing, MI, USA, since 2013.

Peng Zhang was born in Xian, China, on October 20, 1972. He received the M.D. degree and diploma from the Xi'an Jiaotong University College of Medicine, Xi'an, China, in 1994, and the Ph.D. degree in surgery from the Fudan University College of Medicine, Shanghai, China, in 1999.

He was a Postdoctoral fellow in the Department of Surgery at the University of Kentucky, Lexington, KY, USA, from 1999 to 2001 and in the Department of Surgery at the University of California at San Francisco, CA, USA, from 2001 to 2002. He is currently a Professor and a Vice Chair of Surgery, the Founding Director of the Center for Medical Research and Innovation at Shanghai Pudong Hospital and Fudan University Pudong Medical Center, Shanghai. Besides his clinical practice in bariatric surgery, his research interests include etiology, mechanism, diagnosis, and innovative treatment of diabetes and obesity.

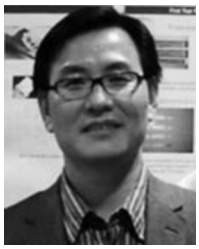

Lirong Zheng (M'01) received the Ph.D. degree in electronic systems design from the Royal Institute of Technology (KTH), Stockholm, Sweden, in 2001.

He is a Professor Chair in media electronics with the KTH, a Founder and the Director of iPack VINN Excellence Center, and a Senior Specialist of Ericsson Networks, Stockholm. Since then, he was at KTH as a Research Fellow and a Project Leader with the Laboratory of Electronics and Computer Systems. He became an Associate Professor in electronic systems design in 2003 and a Full Professor in media electronics at KTH in 2006. He has been a Guest Professor with the State Key Laboratory of ASICs and Systems, Fudan University, Shanghai, China, since 2008, and a distinguished Professor of Fudan University since 2010. He has authored or coauthored more than 200 international reviewed publications, covering areas from electronic devices and thin film technologies, VLSI circuit and system design, to electronic systems and wireless sensors.

His current research interests include electronic circuits and systems for ambient intelligence and media applications, wireless SoC/SiP for sensing and identification, and signal integrity issues in electronic systems.

Hao Min (M'09) was born in Kunshan, China, on July 7, 1965. He received the Ph.D. degree from Fudan University, Shanghai, China, in 1991.

During 1995–1998, he was a Visiting Associate Professor at Stanford University, Stanford, CA, USA, focusing on CMOS image sensors technologies. Meanwhile, he was a Consultant at a number of IC design companies in Silicon Valley. From 1998 to 2005, he served as the Director of the State Key Laboratory of ASIC & System, Fudan University, where he is currently the Director of the Auto-ID Lab. He was General Manager of Shanghai Huahong Integrated Circuits Co., Ltd. during 1998–2006, where his team developed the first contact-less smart card chip, which was successfully applied to the Shanghai Public Transportation System and designed the chip for the second generation ID cards of China. He is the Cofounder of Shanghai Quanray Electronics.

His research interests include SoC Architecture, software-defined technologies, integrated transceiver design, such as RFID, Zigbee, GSM/TDS-CDMA, RF/analog mixed signal integrated circuits design, nonvolatile memory design, digital signal processing, and Image processing. He has contributed more than 80 papers and more than 20 patents authorized or pending.